

The submitted manuscript has been authored by a contractor of the U. S. Government under contract No. W-31 109-ENG-38. Accordingly, the U. S. Government retains a nonexclusive, royalty-free license to publish or reproduce the published form of this contribution, or allow others to do so, for U. S. Government purposes.

## HEATUP OF THE TMI-2 LOWER HEAD

DEC 13 1989

## DURING CORE RELOCATION

CONF-891103--61

DE90 003778

S. K. Wang, J. J. Sienicki, and B. W. Spencer  
Argonne National Laboratory  
9700 South Cass Avenue  
Argonne, IL 60439, USA  
(312) 972-4539

## ABSTRACT

An analysis has been carried out to assess the potential of a melting attack upon the reactor vessel lower head and incore instrument nozzle penetration weldments during the TMI core relocation event at 224 minutes. Calculations were performed to determine the potential for molten corium to undergo breakup into droplets which freeze and form a debris bed versus impinging upon the lower head as one or more coherent streams. The effects of thermal-hydraulic interactions between corium streams and water inside the lower plenum, the effects of the core support assembly structure upon the corium, and the consequences of corium relocation by way of the core former region were examined.

It was found that for the best estimate case in which the corium entered the lower plenum by draining over a major portion of the circumference of the core former region, the corium is calculated to undergo extensive breakup to form a debris bed. The formation of such a debris bed avoids the prediction of any significant thermal attack on the penetration welds. However, even if the bounding severe assumption is made that all of the corium entered the lower plenum in the form of a single coherent stream (i.e., jet), the presence of the core support assembly structure would have caused the single corium jet to be ultimately broken up into an assumed minimum of four smaller streams. (A mechanistic treatment would likely yield a greater number of streams.) For the resulting impingement of the assumed four jets draining from the elliptical flow distributor plate, no melting attack is predicted for the vessel lower head. For this case, the temperature at the vessel wall inner surface is calculated to attain a maximum value of 1200 K remaining well below the material melting temperature ~1800 K.

## NOMENCLATURE

A - area,  $m^2$   
 $C_D$  - drag coefficient  
g - gravitational constant,  $m/s^2$

$h_{fg}$  - latent heat of evaporation, J/kg  
k - thermal conductivity,  $W/m \cdot K$   
k - wave number  $1/m$   
L - length, m  
m - mass, kg  
 $\dot{m}_i$  - mass flux of steam condensation,  $kg/m^2 \cdot s$   
P - pressure, MPa  
 $q_s^*$  - heat flux from structure,  $W/m^2$   
R - jet radius, m  
 $R_v$  - universal gas constant,  $R_v = 8.3 \times 10^{-6}$   $MPa \cdot m^3/gmole \cdot K$   
t - time, s  
T - temperature, K  
U - velocity,  $m/s$   
V - volume,  $m^3$   
w - mass flow rate,  $kg/s$   
z - distance, m

Subscripts

l - liquid (water)  
L - leading edge  
J - coherent jet  
v - vapor (steam)  
SAT - saturation

Greek

$\alpha$  - thermal conductivity,  $m^2/s$   
 $\sigma$  - surface tension, N/m  
 $\rho$  - density,  $kg/m^3$   
 $\delta$  - vapor film thickness, m  
 $\mu$  - kinematic viscosity,  $kg/m \cdot s$   
 $\nu$  - dynamic viscosity,  $m^2/s$   
 $\beta$  - thermal expansion coefficient,  $1/k$

## INTRODUCTION

Background

Planning for the removal of the core support assembly (CSA) from the TMI-2 reactor vessel includes the consideration of the accidental dropping of a portion of the CSA structure into the lower head. Of principal interest is the condition of the weldments securing the incore

instrument nozzles to the lower head vessel wall. If a weldment were to fail during a load drop event, the consequence could be a drainage of water from the reactor vessel. Concern for the integrity of the penetration welds arises from the presence of corium debris inside the lower head. Heat transfer from molten corium during the accident was a potential means of heating up and melting the weld material such that the weldment no longer serves to adequately secure the incore instrument nozzle to the lower head. Thus, the circumstances under which the corium relocated into the lower head and the physical state of the corium when it came into contact with the lower head wall or the individual weldments is of major significance.

According to current perception of the TMI accident, corium largely relocated into the lower head at approximately 224 minutes into the accident.<sup>1</sup> To threaten the weldment integrity, it is necessary that a significant thickness of the weld be melted and ablated away, or heated to a temperature approaching the melting point. Previous studies of the interaction of corium with the lower head have identified two idealized mechanisms by which failure may occur. The first mechanism is the postulated direct impingement of a stream of molten corium upon a weld as a localized and coherent jet.<sup>2</sup> High heat transfer rates may be calculated inside the impingement zone in which the jet splashes off of the lower head or is redirected to flow horizontally over the underlying substrate. The high impingement region heat fluxes can be predicted to erode the weld thickness over a timescale of a few tens of seconds, unless the mitigative effects of water or structure are taken into account. The second mechanism is the postulated accumulation of a large mass of molten corium atop the lower head and penetration welds.<sup>3</sup> If the removal of energy from such a layer due to quenching by overlying water is ignored, then significant heatup and melting of weldments and the lower head may be calculated. (In fact, the debris at TMI was coolable.) This is a relatively much slower process requiring tens of minutes or more.

There are at least three features of the relocation of corium into the lower head during the TMI-2 accident which help to prevent weldment failure by any of the above-mentioned mechanisms. First, corium draining through the lower head as a jet or series of jets will undergo breakup due to its interaction with water. In particular, the corium is broken up into a dispersion of molten droplets which lose energy by heat transfer as they settle through the water. A corium stream will undergo complete breakup after passing through a suitable depth of water. The specific distance depends upon a number of conditions including the jet diameter, extent of breakup may not be complete. However, in this case, the breakup processes still tend to reduce the corium mass remaining in the form of a coherent jet.

Secondly, the core support assembly (CSA) beneath the TMI core incorporates three massive plate members referred to as the flat distributor plate, the lower grid forging, and the elliptical distributor plate. The holes penetrating the lower grid forging and the elliptical plate are not coincident and do not provide a straight-shot pathway from the core to the vessel bottom. As a molten corium stream impacts upon a particular plate, it will tend to splash and spread over the plate and drain through the nearby holes. These processes and the CSA configuration tend to break up a single stream into several streams and enhance the breakup of streams into droplets. Because of the presence of the CSA, which has been observed to be essentially intact in defueling examinations,<sup>4</sup> it is very unlikely that the corium would drain as a single coherent stream from the elevation of the bottom of the core to the lower head vessel wall.

Thirdly, the TMI defueling examinations have revealed that the corium relocated from the molten core region to the lower head predominantly by way of the core former region (CFR) located between the vertical baffle plates immediately surrounding the fuel assemblies and the core barrel. Corium was observed to have spread horizontally within the CFR with solidified debris found over approximately three-fourths of the CFR circumference.<sup>5</sup> The principal pathways for downward flow through the horizontal former plates are the eighty relatively small diameter (3.33 cm) flow holes through each former plate. Consequently, corium drainage from the CFR was likely distributed over a large number of flow holes. In particular, the corium did not exit from the CFR in the form of a single coherent jet. The smaller diameter streams draining from the flow holes will break up more readily giving rise to droplet formation and freezing, and debris bed formation.

The present analysis is concerned with the conditions of the corium as it accumulated inside the lower head during the TMI relocation event which occurred at about 224 minutes into the accident. Current state-of-the-art calculations of the interaction of corium with water in the lower head were carried out consistent with the TMI system configuration and the data recorded during the accident. The heatup of the lower head wall was calculated.

#### Approach

It was found useful to perform calculations for three cases which correspond to the three modes of the TMI corium relocation discussed above.

- 1) A scoping calculation was carried out to ascertain the effects of water alone. This calculation bears no relation to reality because it does not account for the effects of the core support assembly structure or the spreading flow of corium inside the core former region. Instead,

all of the corium is assumed to drain downward as a single jet. Only the effects of the interaction of the corium jet with surrounding water are modeled as a breakup mechanism. The purpose of this calculation is to enable quantification of the mitigative effect of the arduous drainage pathway.

- ii) A bounding severe case in which corium is assumed to drain from the CFR at a single nonvarying location in the form of a localized jet. However, the effects of the CSA in breaking up the corium into several streams as it successively drains through the various plates are modeled. The interactions of each corium stream with water are included.
- iii) A best estimate case in which the lateral spreading of corium within the CFR is accounted for. The corium is assumed to drain simultaneously through the flow holes in the bottom most horizontal core former plate to enter the underlying water in the lower head. Specifically, corium is assumed to drain over a maximum of three-fourths of the circumference of the CFR as observed in TMI defueling examinations. The effects of the CSA as modeled in Case ii were unnecessary owing to the extensive breakup and quench in this case. Jet breakup is due solely to the simultaneous interaction with water of all of the corium streams draining from the flow holes.

In carrying out the analysis, input to the calculations has been selected to be consistent with what is currently known about the TMI-2 accident. In some instances, it has been necessary to estimate conditions inside the reactor vessel. Of specific importance here is the temperature of water residing in the lower head at the time of the relocation event. The dependency of the subcooling upon uncertainties in thermal-hydraulic processes prior to the relocation event was scoped. In determining the subcooling, use was made of the recorded primary system pressure as well as the recommended flowrate and temperature of water delivered by the high-pressure injection capability of the makeup pumps.

A summary of the accident data, estimates of in-vessel conditions, and assumptions incorporated in the analysis is presented in Section II. The results of the corium jet breakup calculations for the three cases are discussed in Section III. Also included here is a comparison of the predicted pressurization of the primary system reflecting net steam formation from the calculated corium-water interactions during the relocation event versus the measured pressures. The calculations of the heatup and potential ablation of the lower head in the presence of an impinging corium jet are presented in

Section III. Overall conclusions and observations are discussed in Section IV. The thermophysical properties for the corium and the vessel lower head are documented in Appendix A and Appendix B, respectively.

#### TMI-2 MOLTEN CORE RELOCATION PHENOMENA AND CONDITIONS

##### Summary of Relocation Event

According to current perception of the TMI-2 accident, at 224 minutes after the turbine tripped, approximately  $25 \times 10^3$  kg<sup>1</sup> molten fuel material (referred to as corium) relocated from a pool contained by a surrounding crust into the vessel core former region (CFR) and the lower plenum. The probable flow path for the molten corium was to impinge upon the vertical baffle plate structure surrounding the core. Following the breaching of the baffle plate, corium which flowed through a hole in the baffle plate to enter the CFR would accumulate upon the horizontal core former plate immediately below the breach. A recent inspection<sup>4</sup> inside the CSA revealed that as much as  $-4.2 \times 10^3$  kg of debris may be in the region between the core barrel and core former baffle plates. Presumably, the remaining  $-20 \times 10^3$  kg of molten corium drained through the core lower structure and collected on the vessel lower head.

It is believed that failure of the crust in the southeast quadrant of the core permitted molten corium to flow out of the pool and impinge upon the vertical baffle plates surrounding the core. Observations from the defueling operations revealed that the R6, P5, and P4 baffle plates (see Figure 6 for core coordinates) are missing, presumed melted, in the region below former plate #5 to midway between former plates #6 and #7. As the depth of the molten corium layer increased, the corium then proceeded to spread laterally over the former plate under the influence of gravity. However, the extent of corium spreading would be restricted by drainage through the flow holes in the core former plate. In particular, each former plate contains eighty circular holes each having a diameter of 1 5/16 inch (3.33 cm). Evidence shows that approximately three-fourths of the CFR circumference were covered by solidified debris. Ultimately, corium drained through the peripheral part of the lower ribbed grid plate to enter the lower head region interior to the CSA. Examination of the CSA structure has shown the presence of corium over a similar extent of the vessel circumference.

In order to assess the vessel heatup and possible ablation due to the impingement of the relocated core material, various postulated relocation paths are assumed and analyzed. The breakup and quench of corium jets draining through different relocation paths and the following thermal attack on the vessel lower head are discussed in Section III. An attempt was made to assess the relocation behavior by comparing the calculated

pressurization rate during the relocation event with the TMI reported measurements.

### Initial Conditions of Corium Jet/Water Interaction

#### Initial Temperature of Corium Jet

Based on the overall energy balance between the heat production rate of a molten fuel pool and the heat loss rate of the pool to its hemispheric crust, the nominal corium superheat immediately prior to the relocation event was estimated to be ~200 K.<sup>6</sup> Thus, an initial temperature of 3050 K was assumed for the corium jet relative to the corium liquidus temperature of 2850 K.

#### Duration of Corium Relocation

As shown in Figure 1,<sup>7</sup> the source range monitor (SRM) response, reactor coolant system (RCS) pressure response, and measured cold leg temperatures all indicated that a global change in the core and reactor vessel conditions occurred over a time span estimated to be 30 to 120 seconds. For an assumed jet diameter, the velocity of the impinging corium stream depends on the relocation time. Based on a hydrodynamic/thermal model of jet breakup as described in Appendix C, the jet velocity strongly characterizes the jet breakup behavior such as the steam generation during corium-water interaction and a concomitant increase in the primary system pressure. It is believed that the SRM response is a direct indicator of change in the core configuration since the SRM directly measures neutron leakage from the core region. According to Figure 1, a significant increase of the SRM count rate occurs at 224.25 minutes and reaches its maximum at 225.75 minutes, and then indicates a normal decay profile. Therefore, the corium relocation time was estimated to be 90 seconds. This value was assumed in the current analysis.

#### Initial Water Temperature and Water Inventory in Vessel Lower Head

During the time interval between when the turbine tripped and the B-loop pump started at 174 minutes of the TMI-2 accident, about half of the primary system coolant was lost to the containment through the stuck open PORV on the pressurizer.<sup>8</sup> The core water level at 174 minutes was estimated to be 0.5 to 1.0 m above the bottom of the active core,<sup>9</sup> and the water temperature was very likely saturated (560 K) based on the hot leg and cold leg water temperature data.<sup>10</sup> At 200 minutes, the high-pressure injection (HPI) system was actuated for approximately 17 minutes. The onset of HPI provided a strong condensation and cooling source within the cold legs and caused the primary system pressure to decrease rapidly as shown in Figure 2. As a result, the pressurizer drained water into the A-loop hot leg and into the

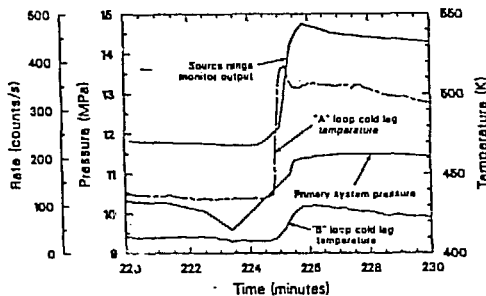


Figure 1. TMI-2 Recorded Data

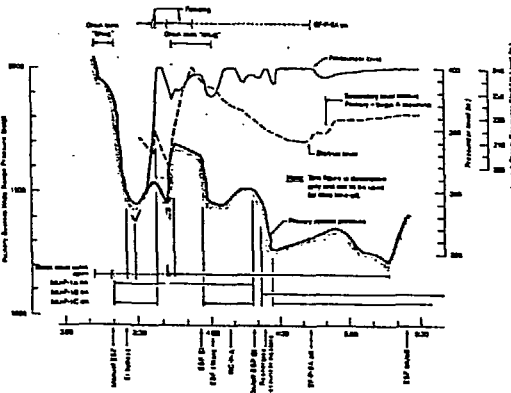


Figure 2. Correlation of Events 3:30 to 5:30

core.<sup>8</sup> Since the temperature of HPI water was much lower (~294 K), the core water would be subcooled which significantly influences the steaming rate and vessel pressurization during the corium relocation. In order to estimate the water temperature in the vessel lower head, the HPI water temperature transient was analyzed based on the recorded pressure data and the recommended HPI injection rates. Assuming that the steam/hydrogen mixture behaves as a perfect gas during the injection of HPI water, then the pressure transient can be related to the condensation rate and volume change rate as expressed below:

$$\frac{\partial P}{\partial t} = \left( \frac{\partial m}{\partial t} \right) \frac{R}{v} T - \frac{P}{v} \frac{\partial v}{\partial t} \quad (1)$$

The change of the volume of steam/hydrogen mixture in the primary system can be calculated based on the flow rate of HPI and the water level in the pressurizer, i.e.,

### DISCLAIMER

This report was prepared as an account of work sponsored by an agency of the United States Government. Neither the United States Government nor any agency thereof, nor any of their employees, makes any warranty, express or implied, or assumes any legal liability or responsibility for the accuracy, completeness, or usefulness of any information, apparatus, product, or process disclosed, or represents that its use would not infringe privately owned rights. Reference herein to any specific commercial product, process, or service by trade name, trademark, manufacturer, or otherwise does not necessarily constitute or imply its endorsement, recommendation, or favoring by the United States Government or any agency thereof. The views and opinions of authors expressed herein do not necessarily state or reflect those of the United States Government or any agency thereof.

$$\left. \frac{\partial \bar{V}}{\partial t} - \frac{\partial \bar{V}}{\partial t} \right|_{\text{HPI}} + \left. \frac{\partial \bar{V}}{\partial t} \right|_{\text{pressurizer}} \quad (2)$$

The estimated HPI injection rate of 60.5 kg/sec as recommended in Reference 11 was assumed. The pressurizer water level is also shown in Figure 2.

During the first seven minutes of HPI injection, the strip chart record of the primary system pressure indicates that the pressure dropped about 400 psi, i.e., an average depressurization rate of about -7.56 kPa/sec. Therefore, the steam is condensed at a net rate of -7.8 kg/sec during this period according to Equation (1). However, the steam condensation due to the HPI injection and the steam generation due to flashing and core steaming all contribute to the net steam condensation rate, i.e.,

$$\frac{\partial m}{\partial t} = \left. \frac{\partial m}{\partial t} \right|_{\text{condensation}} + \left. \frac{\partial m}{\partial t} \right|_{\text{flashing}} + \left. \frac{\partial m}{\partial t} \right|_{\text{core steaming}} \quad (3)$$

Assuming thermodynamic equilibrium and saturation conditions, the average flashing rate due to the depressurization during this period is estimated to be 11.0 kg/sec. The steaming rate due to the boiling off the surface of the degraded core debris, which is believed to have a hemispherical shape with a crust boundary (see Ref. 1), is estimated using the Zuber flat plate critical heat flux expression:<sup>12</sup>

$$\left. \frac{\partial m}{\partial t} \right|_{\text{core steaming}} = 0.14 \rho_v \left[ \frac{\sigma g (\rho_l - \rho_v)}{2 \rho_v} \right]^{1/4} A$$

$$= 15 \text{ kg/s} \quad (4)$$

where A is the area of the top of the hemispherical melt region with radius of -1.25m<sup>2</sup>. Therefore, an average condensation rate due to the HPI injection is estimated to be -33.85 kg/sec. The HPI water temperature immediately prior to entering the vessel lower head can be evaluated based on the calculated HPI condensation rate. Applying mass and energy balance on the control volume of the HPI water as shown in Fig. 3, it yields:

mass equation:

$$w_{\text{out}} = w_{\text{in}} + \int_0^z \dot{m}_i L dz \quad (5)$$

energy equation:

$$\frac{\partial T}{\partial z} = \frac{1}{wC_p} \left\{ \dot{m}_i L [h_{fg} + C_p (T_{\text{SAT}} - T)] + q_s^n L \right\} \quad (6)$$

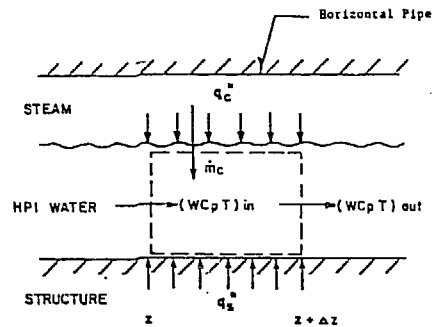


Figure 3 Schematics of HPI Water Heat-up

where

- T = HPI water temperature,
- w = HPI water flow rate,
- l = width of steam/water interface,
- m = mass flux of steam condensation,
- q<sub>s</sub><sup>n</sup> = heat flux from structure, and
- T<sub>SAT</sub> = steam temperature.

The heat flux between the HPI water and structure (i.e., pipe and vessel wall) can be evaluated by assuming transient heat conduction to a semi-infinite region. Thus,

$$q_s^n = \frac{k(T_{\text{SAT}} - T)}{(\pi \alpha t)^{1/2}} \quad (7)$$

where

- t = z/U, and
- U = velocity of HPI water.

Note that the convection heat transfer was neglected since the Biot number is very small. The HPI flow rate is -15 kg/sec (per leg). The water stream is estimated to attain a depth of 8 cm, a width L ~20 cm, and a velocity U ~1 m/sec in the cold legs. When the HPI water stream enters the downcomer, the stream would impinge upon the core barrel and fall along it as an attached film flow. However, there are twenty clips (obstacles) attached to the core barrel to support the upper end of the thermal shield.<sup>13</sup> The HPI water draining down the barrel would be spread laterally by those clips. Based on the orientation of these clips, a width L ~1 m is estimated for the film flow on the core barrel. Equations (5) and (6) were solved to yield the HPI temperature transient on the cold leg and along the downcomer. Figure 4 shows that the HPI water temperature increases by -150 K when it enters the vessel lower head and mixes with the vessel water. Also Fig. 4 shows that the HPI water temperature is not sensitive to the heat conducted from the structure.

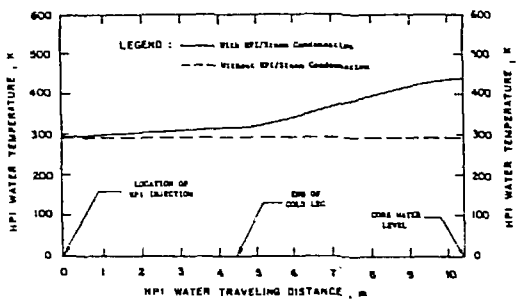


Figure 4. HPI Water Heatup

At 207 minutes when the pressurizer stopped draining, the primary system pressure began to rise. This is a direct result of the reduced HPI-induced steam condensation due to the water level rising above that of the primary piping nozzles and preventing steam from entering the cold legs from the vessel upper plenum.<sup>8</sup> As a result, the cold legs accumulated hydrogen to essentially offset the condensation of steam. The HPI water temperature under this condition, i.e., no HPI/steam condensation, is estimated to increase only slightly as shown in Figure 4. The true HPI water is believed to fall within these two bounding cases.

When the HPI water enters the vessel lower head, it may mix with the water in the lower head. If water is homogeneously mixed in the lower head, water subcooling is calculated to be -90 K. A microscopic investigation of the condensations between water and steam/hydrogen mixture shows a water subcooling ranging from 160 K to 200 K was possible in the TMI lower head after the HPI water injection.<sup>13</sup>

#### CORIUM JET BREAKUP AND TRANSIENT HEATUP OF VESSEL LOWER HEAD

In this section, the breakup of a corium jet (or jets) and temperature transient of the vessel wall will be analyzed and discussed based on the possible relocation paths and jet initial conditions as described in Section II. The vessel heatup is then calculated based on the physical conditions of the impinging jet (i.e., jet temperature, jet velocity, jet diameter, etc.). In order to assess the thermal transient of the vessel wall during the core material relocation, two existing models developed at Argonne National Laboratory have been employed for these analyses. The models which are based upon data obtained from previous experiments carried out at ANL involve: i) the breakup and quench of jets of molten core materials flowing through subcooled (and saturated) water in a film boiling regime, and ii) the convective heat transfer for a jet of corium impinging on a steel surface.

#### Assumed Pathways of Corium Relocation

The breakup and quench of jets of molten core materials are analyzed based on the following assumed relocation paths:

##### Case 1

This is a scoping case to assess the effects of water alone. A 6-inch (0.1524-meter) diameter corium jet is assumed to drain from the lower ribbed grid plate at the location below the lowest former plate as shown in Figure 5. The initial jet velocity is estimated based on the duration of injection as described in Section II. The vessel lower head will suffer a highest thermal attack resulting from relocation of corium through this path due to the melt physical configuration plus neglecting the mitigative effects of the CSA. As described in Section II, the water level was located above the core at the time of the relocation event. Specifically, water will be present when corium first enters the CFR. Subsequently, water may be expelled from the former region in the vicinity of the baffle breach and regions of greater corium accumulation (e.g., on a lower grid rib) due to vigorous steam generation in these regions. As a result, a further breakup and quench of the molten corium in these regions is not likely to occur. Thus, the corium jet is assumed to commence its interaction with water immediately beneath the lower ribbed grid plate as shown in Figure 5.

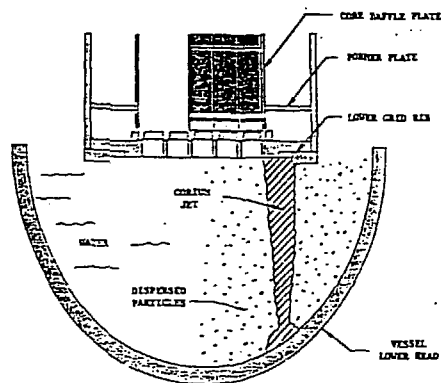


Figure 5. Schematics of Corium Relocation Ignoring Presence of Core Support Assembly (Case 1)

##### Case ii

Case ii is similar to Case i except the effects of the core lower structure on the corium jet breakup are considered. As shown in Figure 6,

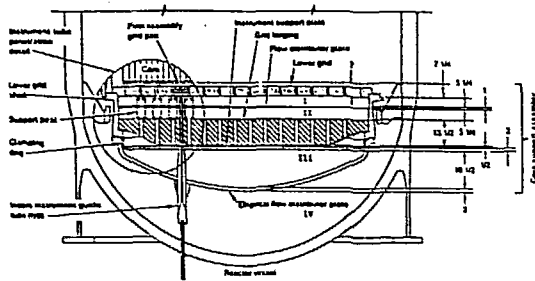


Figure 6. Details of Core Support Assembly Structure

significant interaction with the water is expected to occur in regions I, II, III, and IV. Molten corium is assumed to reaggregate and form multiple jets after it went through regions I, II, and III. Similar to Case i, a 6-inch (0.1524-meter) diameter jet is drained from a 6-inch (0.1524-meter) hole on the lower ribbed grid plate at location R5 as shown in Figure 7. Molten corium accumulates on the flow distributor plate, reagglomerates, and forms four 3 1/2-inch (0.089-meter) diameter jets and one 2 1/2-inch (0.0636-meter) diameter jet. Similar processes of reagglomeration occur on the upper surface of the grid forging and the elliptical flow distributor plate as shown in Figures 8 and 9. A "straight-through" jet cannot exist in this geometry as shown in these figures. The thermal attack upon the vessel lower head will be calculated based on four jets draining from the elliptical flow distributor plate. Due to the pre-fragmentation and multiple jets configuration, the corium streams will suffer more hydrodynamic dispersion and lose more energy prior to impinging upon the vessel lower head. Therefore, relocation of the corium through this path will produce a less conservative yet more realistic thermal load on the lower head than case (i).

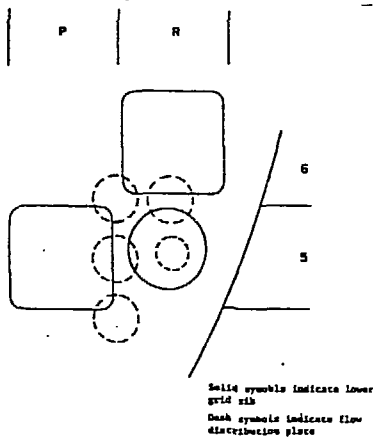


Figure 7. Top View of Lower Grid Rib and Flow Distribution Plate Associated with Corium Relocation (Case ii)

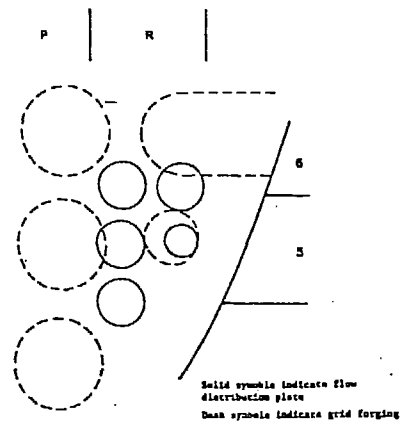


Figure 8. Top View of Flow Distribution Plate and Grid Forging Associated with Corium Relocation (Case ii)

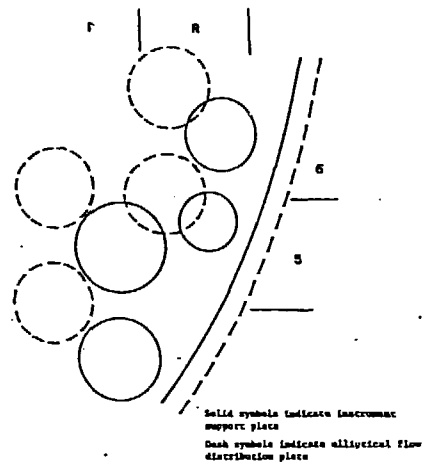


Figure 9. Top View of Instrument Support Plate and Elliptical Flow Distributor Plate Associated with Corium Relocation (Case ii)

Case iii

This is the best estimate case of the relocation based on the evidence of the in-vessel investigation. Examination of the core former region has revealed debris solidified between the lower core former plates over about three-fourths of the circumference of the core barrel. Additionally, examination of the core support assembly structure has shown the presence of corium over a similar extent of the vessel circumference. Therefore, it is plausible to assume that the corium drained through sixty of the eighty holes on the lowest former plate into the vessel water as multiple jets. Since the jet size is small (1 5/16 inch [0.033 meter] diameter), a complete jet breakup was calculated, and the additional dispersion by the CSA structure was thereby neglected.

## Corium-Jet Breakup and Quenching

Based on the experimental results of the corium/water mixing (CCM) tests carried out at ANL,<sup>14</sup> a phenomenological model has been developed to describe the thermal and hydrodynamic behavior of a high-temperature corium jet when it interacts with water in a film boiling regime. A description of this model is presented in Reference 15 and Appendix C. The jet-breakup behavior, such as the mass of corium eroded, the dispersed particle size, etc., is evaluated based on the steam generated from the vaporization of water at the vapor/water interface. The heat transfer aspects of the corium/water interaction, such as the heat transfer coefficient, vapor film thickness, vapor velocity in the vapor film, etc., are solved analytically from the mass, momentum, and energy equations governing the corium/vapor/water interactions. The jet-breakup and quenching behavior predicted by the model has been justified by comparison with measured melt quench/steam generation data from the NRC-sponsored CCM tests, and good agreement has been confirmed.

The predicted behavior of the corium jet breakup and quenching of the TMI-2 core materials during relocation is presented below for the three cases considered. The water subcooling has two major effects on the system pressure in the model: i) it reduces the net steam generation owing to condensation, and ii) it reduces the rate of droplet disengagement from the melt stream (i.e., increases the jet-breakup length) due to the reduced steam interfacial velocity. A higher water subcooling will thereby also increase the corium mass arriving at a surface as a coherent jet owing to the reduction of breakup. Thus, value of higher water subcooling will result in larger calculated convective heat flux of the impinging corium jet on the vessel bottom surface. However, the corium jet may also lose more energy during its travel through the water due to a higher heat transfer into the subcooled water, and this ameliorates the impingement heat flux.

The comparison of measured and predicted system pressure rise attributable to net steam generation is shown in Figure 10. Case i predicts the lowest system pressure rise while Case iii predicts the highest system pressure rise owing to the effects of the largest jet surface area in the latter case. Unfortunately, the uncertainties in the water subcooling preclude the direct use of the pressure measured during the relocation event to select among the various mechanisms. Figures 11 to 13 show the mass of a coherent jet (or jets), the formation of molten droplets, and the solidified droplets (particles) as a function of the jet traveling distance. As predicted by the jet breakup model, the multiple 1 5/16-inch (0.033-meter) diameter jets will breakup completely into quenched

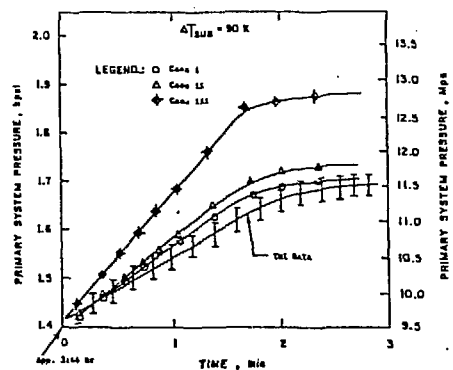


Figure 10. Primary System Pressure (Case i, ii, and iii) for 90 K Water Subcooling

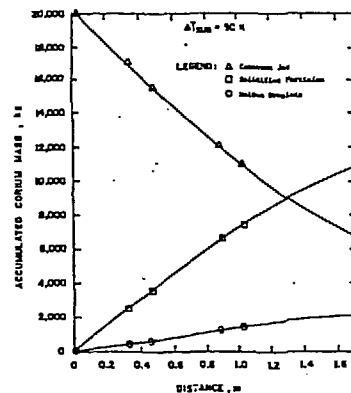


Figure 11. Corium Jet Breakup and Particle/Droplet Formation for Case i

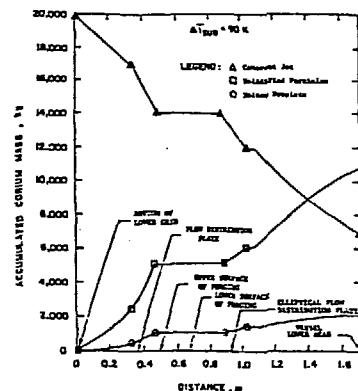


Figure 12. Corium Jet Breakup and Particle/Droplet Formation for Case ii

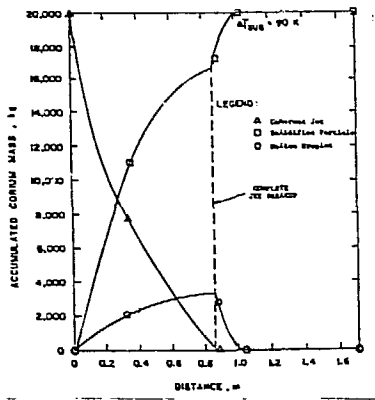


Figure 13. Corium Jet Breakup and Particle/Droplet Formation for Case iii

particles before they reach the vessel head surface. Both Case i and Case ii predict roughly one-third of the total corium mass impacts on the vessel head surface as a coherent jet (or jets). The vessel head heatup was evaluated for Case i and Case ii and the results are presented in the next subsection. Figures 14 to 16 show that the corium temperatures at the various structures. Thus, the ablation of the CSA due to the corium relocation may be possible.

The size of dispersed particles predicted by the jet breakup model ranges from -1 mm to -10 mm with more than 50% of the total dispersed particles less than -2 mm.

#### Heatup of the Lower Head

The impingement of a corium jet upon the lower head may be calculated to result in high heat transfer rates into the steel surface inside the impingement zone in which the corium impacts upon the steel surface and either splashes off of the surface or is redirected to flow horizontally over the surface. The current analysis thus considers the heat transfer phenomena in the impingement region which is expected to represent the greatest potential for thermal attack upon the lower head and failure of the weldment securing one of the instrument penetrations to the vessel wall inner surface. In particular, the temperatures inside the lower head thickness beneath the impingement zone are expected to exceed those in the surrounding regions. Accordingly, the current calculations predict the temperatures across the thickness of the lower head directly beneath the impinging corium and, in the event that melting occurs, the maximum thickness of material which is ablated away. The transient temperatures within the lower head and the ablation rate are calculated using the one-dimensional MISTI computer code previously developed at Argonne National Laboratory. MISTI was originally used for analysis of the Corium Structure Thermal Interaction (CSTI) and Corium Water Thermal Interaction (CWTI) experiments<sup>16</sup> in

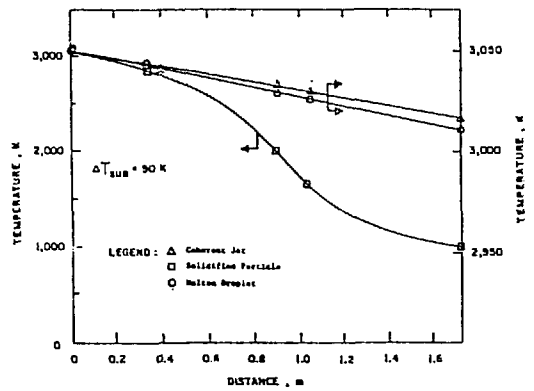


Figure 14. Corium Temperature Variation for Case i

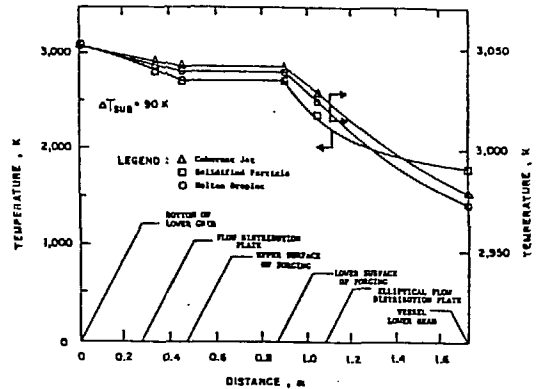


Figure 15. Corium Temperature Variation for Case ii

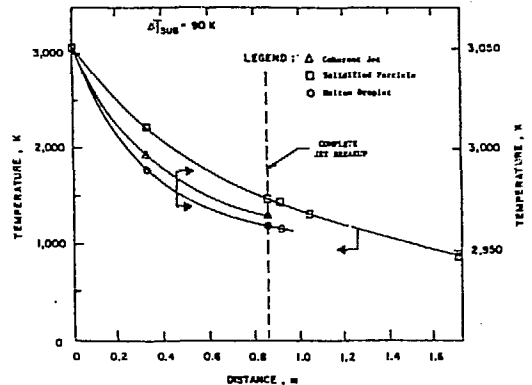


Figure 16. Corium Temperature Variation for Case iii

which predominantly oxide corium mixtures were impinged upon stainless steel plates to provide data on the fundamental mechanisms involved in corium-structure, impingement mode heat transfer. The modeling assumptions and equations currently incorporated in the code are documented in Reference 17. Thermophysical properties employed in the calculations for corium and the lower head are given in Appendices A and B, respectively. A detailed discussion of the thermophysical properties can be found in Ref. 17.

#### Case i (Scoping Calculation)

For the scoping calculation in which a single unimpeded jet is assumed to drain through the lower plenum and the effects of the CSA are unrealistically ignored, the corium jet impinging upon the lower head has a diameter of 8.72 cm, velocity of 1.43 m/sec, and temperature of 3017 K. The corium temperature represents a molten "superheat" of 167 K above the corium freezing temperature of 2850 K. This is the driving temperature difference for heat transfer from the impinging corium stream. For the impinging jet conditions, the forced convection heat transfer coefficient has a value of  $16.0 \text{ kW/m}^2\text{K}$ . This provides a heat flux,  $Q$ , of  $2670 \text{ kW/m}^2$ .

In response to the impingement heat flux, the temperature of the steel at the corium crust-lower head wall interface is calculated to rise to the steel melting temperature of 1810 K over an interval of 37 seconds. This is about one-third of the 90 second duration over which the corium jet is assumed to impinge upon the lower head. The temperature at the corium-steel interface during the pre-melting heatup phase is shown in Figure 17. The temperature profile within the lower head wall at the onset of melting is presented in Figure 18. At this time, the thermal wave has penetrated approximately 7 cm into the steel. Figure 17 also shows the thickness of the interstitial corium crust. The crust thickness rapidly grows to a maximum value of 1.43 mm and then gradually decreases to 0.94 mm as the interface temperature progressively rises to the melting temperature. Thereafter, the crust has a constant thickness as steel ablation is assumed to proceed in a quasi-steady manner. Accordingly, the vessel wall is eroded at a constant rate of 0.331 mm/sec following melting inception. The lower head thickness eroded as a function of time is shown in Figure 19. Over the remainder of the jet impingement interval following the onset of melting, a total erosion of 1.77 cm is calculated. This would be a sufficient thickness to threaten the integrity of a penetration weldment.

#### Case ii (Bounding Severe Calculation)

For the bounding severe case in which a single jet is assumed to drain from the CFR but the effects of the underlying CSA in breaking up the

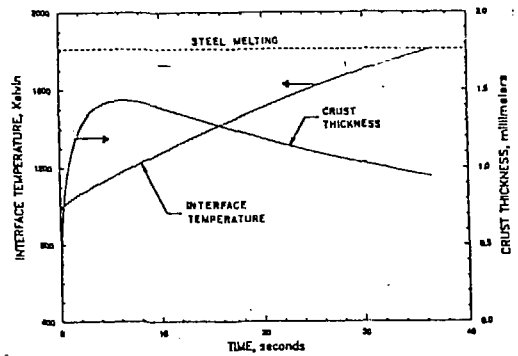


Figure 17.

Temperature at Interface Between Corium Crust and Vessel Lower Head Steel Following Onset of Corium Jet Impingement and Thickness of Corium Crust Formed Upon Lower Head Resulting from the Impingement of a Single Unimpeded Jet.

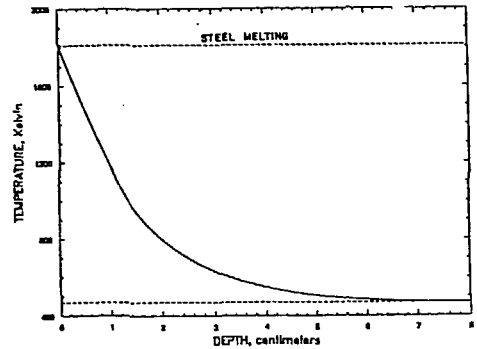


Figure 18.

Temperature Profile Within Vessel Lower Head at the Inception of Steel Melting Resulting from the Impingement of a Single Unimpeded Jet.

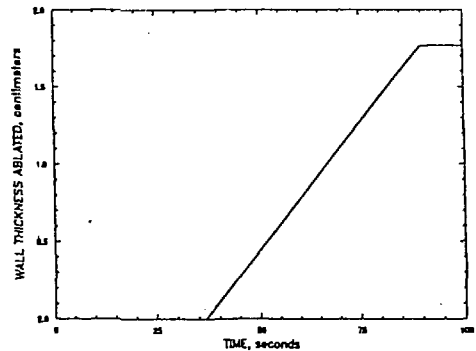


Figure 19.

Thickness of Lower Head Wall Ablated Following Onset of Corium Jet Impingement of a Single Unimpeded Jet.

jet are modeled, the corium is envisioned to impinge upon the lower head as four jets draining from the elliptical flow distributor plate. Because the impinging molten corium is distributed among several jets, the lower head undergoes a heatup which is significantly less severe than that corresponding to the impingement of the corium as a single unimpeded stream. Specifically, the heat transfer effects resulting from the impact of four jets are distributed over a larger portion of the lower head surface and the maximum heat flux into the vessel wall is significantly less than that thus attained with a single unimpeded and localized stream. Similar to the highly conservative scoping calculation, roughly one-third of the corium mass reaches the lower head in the form of the four jets with the remainder having undergone breakup into particles and droplets. It follows that the impingement velocity of each of the four jets is expected to be less than one-fourth of the velocity obtained in the single jet case. In fact, each of the four jets is calculated to impinge with a velocity of 0.251 m/sec versus 1.43 m/sec for the single jet considered previously. The diameter of each impacting stream is 10.7 cm relative to 8.12 cm for the unimpeded stream case. In addition, the corium impinges with a somewhat lower temperature of 2983 K corresponding to a molten superheat of 133 K compared with 167 K of superheat obtained previously. All of these conditions reduce the heat flux inside the impingement zone of each jet. Specifically, the forced convection heat transfer coefficient has a value of 5.60 kW/m<sup>2</sup>\*K and the impingement zone heat flux is equal to 744 kW/m<sup>2</sup> versus 16.0 kW/m<sup>2</sup>\*K and 2670 kW/m<sup>2</sup> for the unrealistic single jet case.

The temperature at the corium crust-lower head wall interface is shown in Figure 20. The temperature is predicted to rise to a maximum value of 1210 K at the end of the 90 second long interval over which jet impingement is assumed to take place. The peak temperature remains 600 K below the lower head melting temperature of 1811 K. Thus, ablation of the lower head is calculated not to occur. The temperature profile through the thickness of the lower head at the end of the jet impingement phase is shown in Figure 21. For the indicated conditions, failure of the weldments securing the instrument penetration guide tubes to the lower head would not be expected.

#### Case iii (Best Estimate Case)

A heatup calculation was not necessary since the corium jets were predicted to breakup into solidified particles with a temperature of ~1000 K (see Fig. 16) when collected upon the lower head.

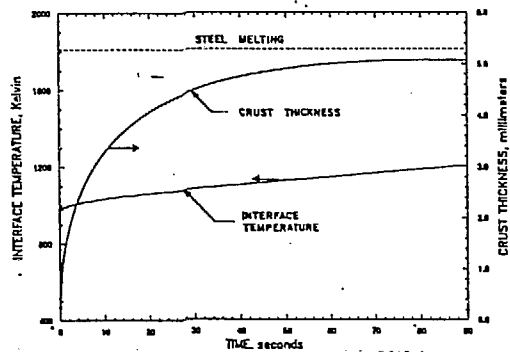


Figure 20.

Temperature at Interface Between Corium Crust and Vessel Lower Head Steel Following Onset of Corium Jet Impingement and Thickness of Corium Crust Formed Upon Lower Head Resulting from the Impingement of Four Corium Jets Draining from the Core Support Assembly.

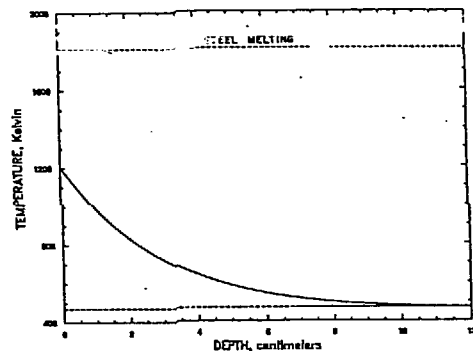


Figure 21.

Temperature Profile through the Thickness of Lower Head at the End of the Jet Impingement Phase.

#### SUMMARY AND CONCLUSIONS

In summary, the following conclusions and observations may be drawn from the current analysis:

- 1) The best estimate case assumes that the corium relocated through the core former region such that corium drained as a large number of jets from the lowermost core former plate. Specifically, the corium is assumed to drain through as many as sixty 3.33 cm diameter flow holes. This corresponds to three-fourths of the circumference of the core former region, consistent with the material dispositions observed in the defueling examinations. Due to interactions with water, the corium jets are calculated to undergo complete breakup into molten droplets which freeze as they settle through the water in the

reactor vessel lower plenum. The predicted particle diameters range from 1 to 10 mm in size. Based upon the results and analysis of the Core Coolant Mixing (CCM) experiments,<sup>18</sup> the debris inside the lower head is predicted to consist of a loose or weakly sintered assemblage of particulates.

- 2) The bounding severe case assumes that the corium enters the lower plenum as a single, coherent, 15 cm diameter jet which drains from the core former region and interacts with the underlying core support assembly structure. The core support assembly causes the original single jet to be broken into multiple jets. For an assumed minimum of four smaller jets impinging upon the lower head, the absence of a melting attack upon the lower head is predicted. In particular, the temperature at the vessel wall inner surface is calculated to attain a maximum value of 1200 K remaining 600 ° below the material melting temperature. Approximately two-thirds of the corium is broken up into droplets ranging in diameter from 1 to 10 mm with the remaining third predicted to impinge upon the lower head as the assumed four jets. Based upon the results and analysis of the Core Coolant Mixing tests, the debris inside the lower head would be predicted to consist of an aggregate mixture of particles and solidified melt.
- 3) Relocation through the core former region has a significant effect in promoting the breakup of corium in water by causing the corium to simultaneously drain from a large number of flow holes as relatively small diameter jets.
- 4) The core support assembly structure has an important effect in protecting the lower head by causing the corium to splash off of the various plates and by breaking up single corium jets into multiple jets. It is impossible for corium to drain through the core support assembly as a single coherent jet.
- 5) Long-term coolability of the debris bed formed in the best estimate case was not examined. It is expected that for the particle sizes calculated to result from the breakup of the corium streams, the bed will be coolable such that no significant heatup of the lower head would subsequently occur.
- 6) A scoping calculation was carried out to ascertain the effects of jet breakup in water alone without the additional breakup effects induced by the core support assembly structure or relocation through the core former region. The corium was assumed to enter the lower plenum as a single, coherent, 15 cm diameter jet.
- 7) The depth of water present between the core and the lower head is not by itself sufficient to protect the lower head without consideration of the additional effects of the core support assembly structure.
- 8) The subcooling of the water in the lower head has a large effect upon the predicted rise in the primary system pressure resulting from interactions of corium with the water. The major effect here is condensation of steam within the bulk water mass. If the water were saturated, the predicted pressure rise would be significantly higher.
- 9) For the best estimate case, subcooling has a minor effect upon the prediction of complete corium breakup. In the severe bounding case, a lower subcooling would have resulted in the calculation of more extensive corium breakup and slightly higher melt temperatures for corium impinging upon the lower head.
- 10) The corium relocation rate was assumed to be uniform over an interval of 90 seconds. This timescale was obtained from the rise time in the count rate of the source range monitor, ex-core, neutron detector. The resulting timescale for the rise in the primary system pressure calculated due to corium-water interactions is in good agreement with the measured pressure data, barring uncertainties in the data reflecting acquisition sampling rates. The use of a shorter relocation time would result in the prediction of a more rapid pressurization than indicated by the data. Similarly, the assumption of a longer relocation interval would give rise to an underprediction of the pressurization rate.
- 11) The modeling of the interactions between corium and water did not account for the possible generation of hydrogen from oxidation of metallic constituents. This is justified in the current analysis because the principal form of the relocated mass was a UO<sub>2</sub>-ZrO<sub>2</sub> mixture.
- 12) The heatup of the lower head was calculated on the basis of impingement of downward directed corium jets. Forced convection

About two-thirds of the corium is calculated to be broken up into droplets. The remaining third is predicted to impinge upon the lower head as a single jet and give rise to ablation of 1.8 cm of the lower head wall thickness. This calculation bears no relation to reality due to the absence of the effects of the core support assembly and spreading flow inside the core former region.

heat transfer inside the impingement zone is expected to represent the highest heat fluxes into the weldments. However, following impingement, the corium might be envisioned to flow laterally along the inner surface of the lower head to impinge upon the neighboring, upright incore instrument nozzles. The prediction of nozzle heatup from this contact mode lies beyond the scope of the current analysis. A major uncertainty here is the potential for a corium jet to splash up off of the lower head surface as opposed to spreading over the surface as a coherent layer.

#### Acknowledgment

The work was funded by the U.S. Department of Energy under DOE Contract DE-AC07-761D01570. This work was performed at the request of General Public Utilities (GPU) Nuclear Corporation. The authors are indebted to GPU Nuclear for their support of this work, and to Mr. Robert Ryan of GPU in particular for his invaluable assistance. The efforts of L. Miller and J. Kawka in preparing the manuscript and figures are deeply appreciated.

#### References

1. "Summary of the TMI-2 Relocation Event," GPU Corp., March, 1988.
2. "Zion Probabilistic Safety Study," Commonwealth Edison Co. (1981).
3. IDCOR 15.2A. Also see "Zion Probabilistic Safety Study," Commonwealth Edison Co. (1981).
4. "U.S. DOE Three Mile Island Research and Development Program 1987 Annual Report," GEND-063, April 1988.
5. J. L. ANDERSON and J. J. SIENICKI, "Thermal Behavior of Molten Corium During the TMI-2 Core Relocation Event," ANS Trans. Vol. 57, p. 429, 1988, also to appear in Nuclear Technology.
6. M. EPSTEIN and H. K. FAUSKE, "The TMI-2 Core Relocation-Heat Transfer and Mechanism," EGG-TMI-7956, July 1987.
7. E. L. TOLMAN et al., "TMI-2 Accident Scenario Update," EGG-TMI-7489, December 1986.
8. R. E. HENRY et al., "Core Relocation Phenomenology," Proceedings of the First International Information Meeting on the TMI-2 Accident," October 21, 1985, Germantown, MD, USA.
9. NSAC-28, "Interpretation of TMI-2 Instrument Data," Nuclear Safety Analysis Center (NSAC), EPRI, March 1980.
10. R. D. MCCORMICK et al., "TMI-2 Data Summary Report," EGG-TMI-7843, September 1987.
11. J. L. ANDERSON, "Recommended HPI Rates for the TMI-2 Analysis Exercise (0-300 Minutes)," EGG-TMI-7833, September 1987.
12. N. ZUBER, "On the Stability of Boiling Heat Transfer," Trans. ASME, Vol. 80, p. 711, 1958.
13. T. G. THEOFANOUS, "The Cooldown Aspects of the TMI-2 Accident," NUREG/CR-4978, August 1987.
14. B. W. SPENCER, J. J. SIENICKI, and L. M. MCUMBER, "Hydrodynamic and Heat Transfer Aspects of Corium-Water Interaction," EPRI-NP-5127, 1987.
15. S. K. WANG, C. A. BLOMQUIST, and B. W. SPENCER, "Modeling of Thermal and Hydrodynamic Aspects of Molten Jet/Water Interactions," ANS Proc. of the 26th ASME/ANS/AICHE National Heat Transfer Conference, Philadelphia, PA, USA, August 6-10, 1989, p. 225-232.
16. J. J. SIENICKI and B. W. SPENCER, "Analysis of Reactor Material Experiments Investigating Corium Crust Stability and Heat Transfer in Jet Impingement Flow," ANS Proceedings 1985 National Heat Transfer Conference, Denver, CO, August 4-7, 1985, p. 255, American Nuclear Society, LaGrange Park, IL (1985).
17. S. K. WANG, J. J. SIENICKI, and B. W. SPENCER, "Assessment of the Integrity of TMI-2 Lower Head Instrument Penetration Weldments," ANL/RAS-GPU-1, August 1988.
18. S. K. WANG, C. BLOMQUIST, B. W. SPENCER, and L. M. MCUMBER and J. SCHNEIDER, "Corium Coolant Mixing Studies," to be published for USNRC.
19. S. K. WANG, C. BLOMQUIST, and B. W. SPENCER, "Interfacial Instability Leading to Bubble Departure and Surface Erosion During Molten Jet/Water Interaction," ANS Proc. of the 26th National Heat Transfer Conference, Philadelphia, PA, August 6-9, 1989, p. 31-38.

## APPENDIX A

## CORIUM PROPERTIES

Corium Composition, wt % UO <sub>2</sub> + 19.7 ZrO <sub>2</sub>	80.3
Corium Composition, mole % UO <sub>2</sub> + 35.0 ZrO <sub>2</sub>	65.0
Liquidus/Freezing Temperature, K	2850
Specific Enthalpy, MJ/kg	
Liquidus	1.50
Solidus	1.13
298 K	0
Heat of Fusion, MJ/kg	0.362
Specific Heat, kJ/(kg·K)	
Liquid	0.565
Solid	0.445
Density, kg/m <sup>3</sup>	
Liquid	7960
298 K	9430
Thermal Conductivity, W/(m·K)	
Liquid	2.88
Solidus	2.88
Viscosity, Pa·s	
3050 K	4.23 x
10 <sup>/3</sup>	
Liquidus	5.31 x
10 <sup>/3</sup>	

## APPENDIX C

MODELING OF THERMAL AND HYDRODYNAMIC ASPECTS  
OF CORIUM JET/WATER INTERACTIONS

Based on the experimental results of the simulant material/water and corium/water tests carried out at ANL, a phenomenological model has been developed to describe the thermal and hydrodynamic behavior of a high-temperature corium jet when it interacts with water.<sup>15</sup> This model can be applied to jets whose diameter is the same order or less than the Taylor wavelength. The jet-breakup length and dispersed-particle-size distribution were analyzed based on Kelvin-Helmholtz instability on the jet column and boundary-layer stripping on the leading edge. The heat-transfer aspects, which strongly affect the jet-breakup behavior, also were analyzed to predict the generation and condensation of steam. The resulting vessel pressurization was estimated and a good agreement between predicted and experimental results was obtained.

## APPENDIX B

## REACTOR VESSEL LOWER HEAD PROPERTIES

Melting Temperature, K	1811
Specific Enthalpy, MJ/kg	
Liquidus	1.29
Solidus	1.05
470 K	0.858
298 K	0
Heat of Fusion, MJ/kg	0.247
Specific Heat, kJ/(kg·K)	
Liquid	0.835
Solidus	0.761
470 K	0.519
298 K	0.450
Density, kg/m <sup>3</sup>	
Liquidus	7010
Solidus	7320
470 K	7810
298 K	7870
Thermal Conductivity, W/(m·K)	
Liquidus	24.1
Solidus	38.6
470 K	41.2
298 K	41.2
Liquidus Viscosity, Pa·s	5.36 x
10 <sup>/3</sup>	

Modeling of Pour-Stream Breakup

Based on the observation of simulant material tests, a conceptual configuration of the jet when it interacts with the water has been assumed as shown in Figure C.1. In high-temperature melt tests, a vapor film is always found to blanket the pour stream and the pour stream is embedded in a highly-voided two-phase mixture as shown in Fig. C.1a. A vortex ball (i.e., the leading edge), followed by a coherent jet column, is usually formed immediately after the jet submerged into the water. As the frontal vortex ball descends in water, its size varies due to material inflow accumulated from the jet trailing column and material erosion by the ambient fluid. A considerable amount of particles, some rather large in size, were detached from the tail of the vortex ball while the particles dispersed from the coherent column seemed to be smaller.<sup>16</sup> Finally, the jet column became symmetrical (varicose) in shape and thinner and eventually jet breakup occurred.

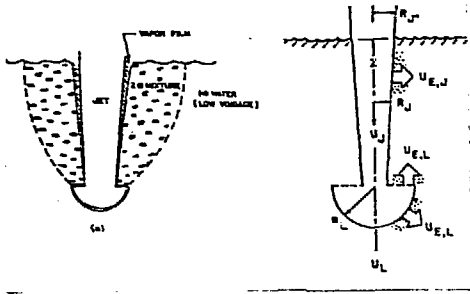


Figure C.1 Schematic Configuration of Jet Breakup

If the erosion of the jet material is characterized by the erosion velocities  $U_{E,J}$  and  $U_{E,L}$  on the jet column and the leading edge, respectively, then the dynamic governing equations of the jet can be obtained by applying mass and force balance on the coherent column and the leading edge as follows:

$$2 \frac{\partial R_J}{\partial t} - U_{E,J}; R_J(o) = R_o \quad (C.1)$$

$$(\rho_m + \rho_l/2) \frac{\partial \left( \frac{U_{L,V}}{L} \right)}{\partial t} - \rho_m \int_0^{R_J(t)} (U_J - U_L) U_J 2\pi r dr$$

$$+ (\rho_m - \rho_l) g \bar{V}_L - \rho_m U_L \frac{\partial V_{E,L}}{\partial t}$$

$$- \frac{1}{2} C_D \rho_l U_L^2 \pi R_L^2; U_L(o) = U_J \quad (C.2)$$

$$\frac{\partial \bar{V}_L}{\partial t} - \int_0^{R_J(t)} (U_J - U_L) 2\pi r dr - \frac{\partial \bar{V}_{E,L}}{\partial t}; R_L(o) = R_J(o) \quad (C.3)$$

The time variations of the jet diameter, the leading-edge velocity, and the leading-edge volume can be determined from these simultaneous differential equations (C.1, C.2, and C.3), if the erosion velocities on the jet column and leading edge (i.e.,  $U_{E,J}$  and  $U_{E,L}$ ) are known. It will be shown later that the erosion velocities depend strongly on the steam generated on the column and leading edge. Therefore, the jet-breakup behavior is coupled with the corium-water thermal interaction.

The Kelvin-Helmholtz instability at the vapor/liquid interface has been discussed by many authors. The fastest growth rate and wave number of the interfacial disturbances were determined by differentiating the dispersion equation. Then the erosion velocity (i.e., the growth rate of the surface disturbance) of the dispersed particles at the interface due to droplet disengagement can be approximated by imaginary part of the velocity of the wave with the fastest growth rate. Wang et al.<sup>19</sup> analyzed an inviscid parallel flow of high-temperature melt and water separated by a thin sheet of steam that could occur during a molten-jet/water interaction. They concluded that the erosion velocity of the particles dispersed from the jet surface is

$$U_{E,m} = \frac{[\rho_v \rho_m (U_v - U_m)^2 - \sigma_m k (\rho_v + \rho_m)]^{1/2}}{K \rho_v + \rho_m} \quad (C.4)$$

where  $K = (1 + \cosh k\delta) / \sinh k\delta$ , and the most probable wave number,  $k_p$ , is:

$$k_p = \frac{2\rho_v U_v^2 K}{3\sigma_m} \quad (C.5)$$

Therefore, the erosion due to Kelvin-Helmholtz instability depends on the vapor (steam) velocity in the vapor film. The erosion on the jet column is assumed to occur solely from this type of instability.

By assuming a linear temperature profile in the vapor film and a parabolic profile for the liquid (water) velocity and the temperature in the liquid boundary layers, as shown in Figure C.2, and applying the integral momentum and energy equations, the vapor-film thickness,  $\delta$ , vapor velocity  $U_v$ , and interfacial velocity  $U_i$  can be determined by solving the following equations:

$$\int_0^\delta \frac{\partial U_v^2}{\partial z} dy - \int_0^\delta U_i \frac{\partial U_v}{\partial z} dy - \int_0^\delta g \frac{\Delta \rho}{\rho} dy + \int_0^\delta K_p (U_p - U_v)^2 dy + \frac{\tau_i}{\rho} + \frac{\tau_w}{\rho} = 0 \quad (C.6)$$

$$\frac{\partial}{\partial z} \int_0^\delta U_l (U_l - U_\infty) dy - \int_0^\delta T \beta_l (T_l - T_\infty) g dy - \nu_l \frac{\partial U_l}{\partial y} \Big|_{y=0} \quad (C.7)$$

$$(q_R^* - k_v \frac{\partial T_v}{\partial y}) - (-k_l \frac{\partial T_l}{\partial y}) = \rho_v h_{fg} \left[ \frac{\partial}{\partial z} \int_0^\delta U_v dy + \frac{U_{E,v}}{2} \right] \quad (C.8)$$

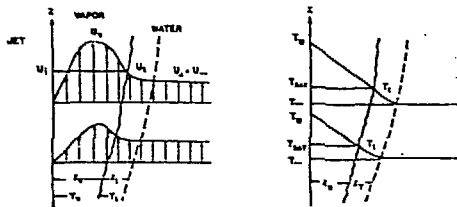


Figure C.2 Velocity and Temperature Profiles on Jet Column

In addition to the surface instability, aerodynamic stripping also accounts for the erosion on the leading edge. Assuming that the corium surface layer of the leading edge is constantly dragged by the enveloping fluid, i.e., steam, and departs from the main body at the tail edge due to an abrupt change in the pressure distribution, and assuming a velocity profile for the surface layer.

$$U_m = U_{ml} \exp \left[ - \frac{y_m}{C \sqrt{x}} \right] \quad (C.9)$$

The velocity and temperature profiles of vapor and liquid adjacent to the leading edge are similar to those of the jet column except  $z$  is replaced by  $x$  and  $g$  is replaced by  $g \sin \theta$ , as shown in Figure C.3. In addition to Equations C.6-C.8, two more equations are needed:

$$\frac{\partial}{\partial x} \int_0^\infty U_m^2 dy_m = \nu_m \frac{\partial U_m}{\partial y_m} \Big|_{y_m=0} \quad (C.10)$$

and

$$\mu_m \frac{\partial U_m}{\partial y_m} \Big|_{y_m=0} = \mu_v \frac{\partial U_v}{\partial y_v} \Big|_{y_v=0} \quad (C.11)$$

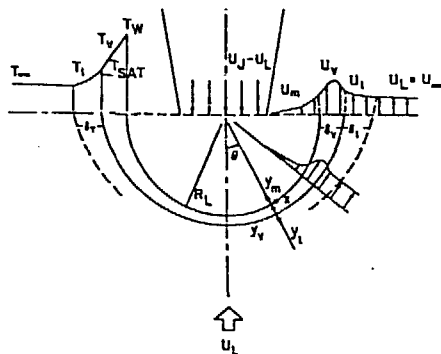


Figure C.3 Film Boiling and Erosion on Leading Edge

The erosion velocity (or the rate change of the volume) on the leading edge can be approximated by:

$$\frac{\partial \bar{V}_{E,L}}{\partial \tau} = \int_0^{R_L} 2\pi R_L U_m \Big|_{\theta=\pi/2} dR_L = 2\pi U_{ml} C_m \frac{\pi R_L}{2} \left[ R_L - C_m \frac{\pi R_L}{2} \right] \quad (C.12)$$

After the erosion velocities on the column and leading edge are calculated, the jet breakup behavior can be completely determined by solving Equations C.1, C.2, and C.3.

#### Dispersed Particle Size Distribution

As described before, the diameter of the particles dispersed from the jet column surface due to Kelvin-Helmholtz instability is approximately by the wavelength of the most unstable wave. Thus,

$$D_p = \frac{1}{k_p} = \frac{3\sigma_m}{2\rho_v U_v^2} \quad (C.13)$$

However, the particles dispersed from the tail of the leading edge may show quite a different size distribution since the erosion mechanism is completely different. Presumably, the drag-induced energy is lost at the tail in the form of the kinetic energy of dispersed particles and the formation of a new surface area. Then the particle size can be estimated by solving the following equation:

$$\frac{1}{2} \rho_m \int_0^{\infty} 2\pi (R_L - y) U_m^3 \Big|_{x=\pi(R_L/2)} dy$$

$$-\frac{6\sigma_m}{D_p} \left( \frac{\partial \bar{V}_{E,L}}{\partial t} \right) + \frac{1}{8} \rho_m U_m^2 \left( \frac{\partial \bar{V}_{E,L}}{\partial t} \right) \quad (C.14)$$

For a thin corium boundary layer, Equation C.14 can be simplified to yield

$$D_p = \frac{144\sigma_m}{\rho_m U_m^2} \quad (C.15)$$

Comparing Equations C.13 and C.15, the dispersed particles of the leading edge are usually -1 to -10 times bigger than the dispersed particles of the jet column during the corium/water interaction.

#### Film Boiling Heat Transfer on Particles

The heat transfer from a descending, dispersed particle is illustrated in Figure C.4. For simplicity, heat conduction is neglected in the trailing vapor dome. The vapor velocity in the vapor film, the film thickness, and the heat transfer coefficient, etc., can be determined by solving the equations similar to Equations C.6-C.8 except the curvature on the particle is considered. The average heat transfer coefficient,  $\bar{h}$ , is approximated by

$$\bar{h} = \frac{1}{4\pi R^2} \left\{ \int_0^{\pi/2} \left( q_R^* - k_v \frac{\partial T_v}{\partial r} \Big|_R \right) 2\pi R^2 \sin\theta d\theta + \int_{\pi/2}^{\pi} q^* 2\pi R^2 \sin\theta d\theta \right\} \quad (C.16)$$